J Neuropathol Exp Neurol
Vol. 80, No. 6, June 2021, pp. 530–540
doi: 10.1093/jnen/nlab040

ORIGINAL ARTICLE

Cytoplasmic Mislocalization of RNA Polymerase II Subunit RPB1 in Alzheimer Disease Is Linked to Pathologic Tau

John R. Dickson, MD, PhD, Hyejin Yoon, PhD, Matthew P. Frosch, MD, PhD, and Bradley T. Hyman, MD, PhD

Abstract

Abnormal protein accumulation and mislocalization is a general hallmark of Alzheimer disease. Recent data suggest nucleocytoplasmic transport may be compromised by tau in Alzheimer disease. In this context, we have examined the RNA polymerase II subunit RPB1, which is the catalytic subunit that plays a critical role in transcription. Using immunofluorescence staining in control and Alzheimer disease hippocampal tissue, we show that 2 phosphoisoforms of RPB1 mislocalize from the nucleus to the cytoplasm of neurons in Alzheimer disease. The number of neurons with this cytoplasmic mislocalization is correlated with the burden of pathologic tau (AT8-immunopositive neurons). In order to test whether there is a causal relationship between pathologic tau and cytoplasmic RPB1 accumulation, we used the rTg4510 mouse model, which expresses a regulatable pathologic human tau species harboring the P301L mutation. Using immunofluorescence staining on brain tissue from young (2.5-month-old) and aged (8.5- to 10-month-old) rTg4510 mice, we found a tau- and age-dependent increase in cytoplasmic mislocalization of Rpb1. In summary, this study provides evidence that tau induces mislocalization of RPB1 in Alzheimer disease, and since RPB1 is essential for transcription, this raises the possibility that RPB1 mislocalization could lead to fundamental alterations in neuronal health.

From the Department of Neurology, MassGeneral Institute for Neurodegenerative Disease, Massachusetts General Hospital, Charlestown, Massachusetts (JRD, HY, BTH); Harvard Medical School, Boston, Massachusetts (JRD, HY, MPF, BTH); C.S. Kubik Laboratory for Neuropathology, Department of Pathology, and Neurology Service, Massachusetts General Hospital, Boston, Massachusetts (MPF).

Send correspondence to: Bradley T. Hyman, MD, PhD, MassGeneral Institute for Neurodegenerative Disease, Department of Neurology, Massachusetts General Hospital, Building 114, 114 16th Street, Charlestown, MA 02129; E-mail: bhyman@mgh.harvard.edu.

This study was supported by the National Institutes of Health (NIH) National Institute of Neurological Disorders and Stroke (NINDS) grant R25NS065743 (JRD). Support was also provided by the JPB Foundation (BTH). The Massachusetts Alzheimer's Disease Research Center is funded by the National Institutes of Health (NIH) National Institute on Aging (NIA) grant 1P30AG062421-01.

The authors have no duality or conflicts of interest to declare.

Supplementary Data can be found at http://academic.oup.com/jnen.

Key Words: Alzheimer disease, RNA polymerase II, RPB1, rTg4510, Tau.

INTRODUCTION

Alzheimer disease is the most common type of dementia and is characterized neuropathologically by abnormal accumulation of 2 proteins: extracellular aggregation of amyloid β and intracellular aggregation of tau (1). The aggregated tau exhibits an altered subcellular localization in Alzheimer disease. Although tau, a microtubule binding protein, is normally localized to neuronal axons (2), the subcellular localization of tau shifts to the somatodendritic compartment in Alzheimer disease (3). While this is a classic pathologic hallmark of Alzheimer disease, protein mislocalization in Alzheimer disease has been reported for other proteins, such as nuclear transport factor 2 (NTF2) (4), Ras-related nuclear protein (RAN) (5), DNA (cytosine-5)-methyltransferase 1 (DNMT1) (6), and DNA-directed RNA polymerase II subunit B1 (RPB1) (6, 7).

RPB1 is the catalytic subunit of RNA polymerase II, which is responsible for the transcription of messenger RNAs (mRNAs) and most small nuclear RNAs and microRNAs in the nucleus (8). The carboxy-terminal domain (CTD) of RPB1 is intrinsically disordered (9) and contributes to the regulation of transcription through post-translational modification of residues in a series of imperfect heptad repeats of amino acids, the consensus sequence of which is YSPTSPS (10). The most common form of post-translation modification is phosphorylation of the serine and threonine residues, with specific phosphorylation states marking specific steps in the process of transcription. Notably, phosphorylation of serine 5 in the heptad repeat is associated with transcription initiation and assists with promotor escape. Phosphorylation of serine 2 in the heptad repeat is associated with transcription elongation and assists with splicing factor recruitment and ultimately transcription termination (10).

In previous studies examining RPB1 in Alzheimer disease, the unphosphorylated CTD is generally not detectable in neurons, suggesting RPB1 is highly phosphorylated in Alzheimer disease. Using phospho-specific antibodies, mislocalization of RPB1 phosphorylated at CTD serine 5 (CTD Ser5P)

© 2021 American Association of Neuropathologists, Inc.
This is an Open Access article distributed under the terms of the Creative Commons Attribution Non-Commercial License (http://creativecommons.org/licenses/by-nc/4.0/), which permits non-commercial re-use, distribution, and reproduction in any medium, provided the original work is properly cited. For commercial re-use, please contact journals.permissions@oup.com

and serine 2 (CTD Ser2P) has been demonstrated in the hippocampus of Alzheimer disease cases (7). Similarly, mislocalization of RPB1 to the cytoplasm of neurons in the cornu Ammonis subfield 1 (CA1) of Alzheimer disease hippocampus was observed using a polyclonal antibody without specificity to a particular phospho-epitope (6).

Since we have recently suggested that alterations in the nuclear pore complex and disruptions in nucleocytoplasmic transport occur in tauopathy models and in Alzheimer disease (5), we were interested in further exploring the cytoplasmic mislocalization of RPB1 in the context of Alzheimer disease and understanding if this mislocalization is a correlate of or a consequence of tau-related pathological changes. Given the essential role of RPB1 in the transcription of mRNA, we were also motivated by recent observations of a general repression of gene expression in neurons in Alzheimer disease prefrontal cortex based on single-nucleus RNA sequencing (11). In postmortem hippocampal tissue from Alzheimer disease and control cases, we confirmed that the number of neurons with cytoplasmic RPB1 CTD Ser5P and RPB1 CTD Ser2P is significantly increased in Alzheimer disease, consistent with previous reports (6, 7). To examine whether tau mediates this mislocalization phenotype, we examined a mouse model of tauopathy with regulatable pathologic tau expression (rTg4510). We found a tau- and age-dependent accumulation of cytoplasmic Rpb1. These results suggest the cytoplasmic mislocalization of RPB1 occurs downstream of pathologic tau in the pathobiology of Alzheimer disease.

MATERIALS AND METHODS

Human Tissue

Age-matched cases of Alzheimer disease or cognitively normal controls (n = 10 per group) were identified in the Massachusetts Alzheimer's Disease Research Center Neuropathology Core (summarized in Table 1, detailed in Table 2), and paraffin-embedded hippocampus samples from each case were sectioned on an RM 2155 microtome (Leica Microsystems, Inc., Buffalo Grove, IL) at the thickness of 7 μm and mounted on Fisherbrand Superfrost Plus Microscope Slides (Thermo Fisher Scientific, Waltham, MA). Fresh frozen hippocampal tissue from an Alzheimer disease case (Arbitrary Case #20, Table 2) was also obtained from the Massachusetts Alzheimer's Disease Research Center Neuropathology Core for validation of antibody specificity by Western blot.

Mouse Tissue

The rTg4510 mouse model expresses human 4-repeat tau with the pathogenic tau P301L mutation under the control of a tetracycline-operon-responsive element, and it expresses the tet-off open reading frame under the control of the Ca^{2+}-*calmodulin kinase II* promotor, which limits expression to forebrain structures. The expression of the tau transgene can be suppressed by administration of doxycycline in this mouse model (12). Archival tissue from a prior study (13) was used for the completion of this study. In brief, young (2.5-month-old) and aged (8.5- to 10-month-old) mice were used in 3 groups: a control group of nontau transgenic littermates that contain only the tet-off open reading frame transgene treated with 200 ppm of doxycycline in food (Bio-Serv, Flemington, NJ) for 6 weeks (n = 3 mice in each age group), rTg4510 mice with suppression of tau transgene expression by administration of 200 ppm of doxycycline in food for 6 weeks (n = 3 mice in each age group), and rTg4510 mice receiving no doxycycline treatment (n = 3 mice in each age group). The rTg4510 mice were randomly assigned to receive doxycycline or no doxycycline treatment. Animals were housed and treated according to institutional and National Institutes of Health standards. Beyond the groups and ages described above, there were no additional inclusion or exclusion criteria utilized in this study. No animals were excluded from the analysis. At the defined age time points, the mice were killed and brains were drop-fixed in formalin and then embedded in paraffin. Parasagittal sections were cut at a thickness of 16 μm on an RM 2155 microtome (Leica Microsystems, Inc.) and mounted on Fisherbrand Superfrost Plus Microscope Slides (Thermo Fisher Scientific).

Antibodies

A complete list of antibodies used is presented in Table 3. All antibodies were aliquoted and stored according to the manufacturers' instructions prior to use.

Antibody Specificity

Dephosphorylation of human brain homogenate followed by Western blot was performed to determine the specificity of RPB1 CTD Ser5P (3E8) and RPB1 CTD Ser2P (3E10) antibodies (MilliporeSigma, Burlington, MA). Fresh frozen hippocampal tissue from an Alzheimer disease case (1500 mg) was homogenized in 150 μL of lysis buffer (20 mM Tris-HCL, pH 7.5, 150 mM NaCl, 1 mM EDTA, 1 mM EGTA, and 1% Triton X-100 with protease inhibitor cocktail [MilliporeSigma]). The lysate was centrifuged at 12 000 × g for 15 minutes to collect the total protein in the supernatant. The protein concentration was determined using the Pierce BCA Protein Assay Kit (Thermo Fisher Scientific). Dephosphorylation of the homogenate was performed by incubated 40 μg of protein with 0, 10, 100, 400, or 2000 units of Lambda Protein Phosphatase (New England Biolabs, Ipswich, MA), 1X NEBuffer for Protein MetalloPhosphatases (New England Biolabs), and 1 mM $MnCl_2$ (New England Biolabs) for 15 minutes at 30°C in a 50 μL reaction. Phosphatase inhibitor cocktail (Thermo Fisher Scientific) was added only to the no phosphatase-treated control. To stop the reaction, the protein mixture was boiled with 1% sodium dodecyl sulfate (Thermo Fisher Scientific), 1X NuPAGE Sample Reducing Agent (Thermo Fisher Scientific), and Fluorescent Compatible Sample Buffer (Thermo Fisher Scientific). For each reaction condition, 8 μg of protein was separated by electrophoresis using a NuPAGE 3–8% Tris-Acetate Gel (Thermo Fisher Scientific) with NuPAGE MOPS SDS Running Buffer (Thermo Fisher Scientific) then transferred to nitrocellulose membrane (Thermo Fisher Scientific) by electroblotting at 40 mA for 12 hours at 4°C. Blots were blocked with Odyssey Blocking Buffer (LI-COR, Lincoln, NE) for 1 hour and then incubated

TABLE 1. Characteristics of Control and Alzheimer Disease Cases.

	Control	Alzheimer Disease	p Value*
Number	10	10	
Number of females (%)	4 (40%)	5 (50%)	
Age at death in years (SD)	76.8 (12.3)	73.9 (14.9)	0.64
PMI in hours (SD)	29.9 (21.2)	17.7 (8.1)	0.16

PMI, postmortem interval.
*Calculated with Welch's *t*-test.

TABLE 2. Details of Cases Included.

Arbitrary Case #	Case Type	Braak Stage	Age	Sex	*APOE* Genotype	PMI
1	Control	NA	60	M	NA	11
2	Control	NA	73	F	ε3/ε3	NA
3	Control	NA	86	M	ε3/ε3	10
4	Control	0	58	F	ε3/ε3	18
5*	Control	I	68	M	ε3/ε3	NA
6	Control	I	76	F	ε3/ε3	48
7	Control	I	77	F	NA	72
8*	Control	II	87	M	ε2/ε3	21
9	Control	II	89	M	NA	36
10	Control	II	94	M	NA	23
11	Alzheimer	I	74	F	NA	19
12	Alzheimer	I	81	M	ε3/ε3	18
13	Alzheimer	III	79	F	NA	6
14*	Alzheimer	III	84	F	ε3/ε3	33
15	Alzheimer	IV	90	M	ε3/ε3	24
16	Alzheimer	VI	51	M	NA	8
17	Alzheimer	VI	54	F	ε3/ε3	16
18	Alzheimer	VI	61	M	NA	18
19*	Alzheimer	VI	70	F	ε3/ε4	24
20	Alzheimer	VI	95	M	ε3/ε3	11

NA, not available; PMI, postmortem interval.
*Due to limited tissue availability, staining for RPB1 CTD Ser2P was not performed on these cases.

with rat anti-3E8 or 3E10 antibody and chicken anti-GAPDH antibody (MilliporeSigma) for 1 hour at room temperature. The blots were washed with tris-buffered saline with 0.1% TWEEN 20 Detergent (MilliporeSigma) (x4, 4 minutes each). The blots were incubated with IRDye 800CW anti-Rat IgG and IRDye 680RD anti-Chicken IgG secondary antibodies (LI-COR) for 1 hour at room temperature and subsequently washed with tris-buffered saline with 0.1% TWEEN 20 Detergent (MilliporeSigma) (x4, 4 minutes each). The blots were imaged using the Odyssey CLx Imaging System (LI-COR).

Immunofluorescence Staining

Paraffin-embedded tissues sections on glass slides were deparaffinized in xylenes (Thermo Fisher Scientific) (x2, 5 minutes each) and rehydrated through sequential incubation in 100% ethanol (VWR International, Radnor, PA) (x2, 5 minutes each), 95% ethanol (x1, 5 minutes), 70% ethanol (x1, 5 minutes), 50% ethanol (x1, 5 minutes), and distilled water (x2, 5 minutes each). Antigen retrieval was performed in IHC-Tek epitope retrieval solution (IHC World, Woodstock, MD) in a humidified chamber at 95–100°C for 1 hour. After cooling on ice for 10 minutes, the tissue was permeabilized in 0.4% Triton X-100 (MilliporeSigma) in phosphate-buffered saline (Thermo Fisher Scientific) for 8 minutes. Blocking was performed with 10% normal goat serum (MilliporeSigma) in phosphate-buffered saline for 1.5 hours at room temperature. Primary antibodies were diluted as indicated in Table 3 in Antibody Diluent (Abcam, Cambridge, UK) and incubated at 4°C overnight. Slides were subsequently washed in 5% normal goat serum and 0.5% Triton X-100 in tris-buffered saline (MilliporeSigma) (x4, 2 minutes each). Fluorescently labeled secondary antibodies were diluted as indicated in Table 3 in Antibody Diluent (Abcam) and incubated at room temperature for 1.5 hours. Slides were then washed in 5% normal goat serum and 0.5% Triton X-100 in tris-buffered saline (x3, 2 minutes each) followed by washes in tris-buffered saline (x2, 2 minutes each). Nuclei were counterstained with 4',6-diamidino-2-phenylindole ([DAPI], MilliporeSigma) diluted 1:1000 in phosphate buffered saline with a 5-minute incubation. Slides were then washed in phosphate buffered saline (x3, 5 minutes each). Tissue autofluorescence was quenched with a solution of 0.1% Sudan Black (MilliporeSigma) in 70% ethanol in a 30-minute incubation. Slides were washed in phosphate buffered saline (x3, 5 minutes each). Gold Seal Cover Glass Coverslips (Thermo Fisher Scientific) were mounted with Fluoromount G with DAPI (Southern Biotech, Birmingham, AL) and sealed with clear nail polish (Electron Microscopy Sciences, Hatfield, PA).

Microscopy

Epifluorescence microscopy was performed using a VS120 Virtual Slide Microscope (Olympus, Tokyo, Japan) with a 40X objective. Confocal microscopy was performed using a FLUOVIEW FV3000 Confocal Laser Scanning Microscope (Olympus) with a 60X oil objective.

Quantification

Using cellSens software (Olympus), a 0.25 μm × 0.25 μm grid was overlaid on the epifluorescence images to assist with quantification. For human brain tissue, the CA1 region of the hippocampus was outlined and every 5th square moving left to right and top to bottom was selected to quantify the number neurons (indicated by MAP2 staining) containing RPB1 in the cytoplasmic compartment. The nuclear compartment was denoted by the DAPI counterstain. The number of neurons staining with the phospho-tau antibody AT8 was also quantified. For mouse brain tissue, a similar quantification method was used, but given the smaller size of the CA1 in mice, all squares containing the CA1 were counted. All tissues were labeled with a number unrelated to diagnosis, genotype, or doxycycline treatment in order to limit bias in the process of quantification. Since the phospho-tau staining pattern with

TABLE 3. Antibodies Used for Immunofluorescence (IF) Staining and Western Blotting (WB).

Antibody	Host	Manufacturer	Catalog #	IF Dilution	WB Dilution
RPB1 phospho-CTD Ser-5 (3E8)	Rat	Millipore Sigma, Burlington, MA	04-1572	1:200	1:1000
RPB1 phospho-CTD Ser-2 (3E10)	Rat	Millipore Sigma	04-1571	1:200	1:1000
Phospho-tau (Ser202, Thr205) (AT8)	Mouse	ThermoFisher Scientific, Waltham, MA	MN1020	1:200	–
MAP2	Chicken	Abcam, Cambridge, UK	ab5392	1:400	–
GAPDH	Chicken	Millipore Sigma	AB2302	–	1:2000
Anti-Rat IgG H&L (Alexa Fluor 555)	Goat	Abcam	ab150166	1:200	–
Anti-Mouse IgG (H + L), Alexa Fluor 488	Goat	ThermoFisher Scientific	A28175	1:200	–
Anti-Chicken IgY (H + L), Alexa Fluor 647	Goat	ThermoFisher Scientific	A32933	1:200	–
IRDye 800CW anti-Rat IgG	Goat	LI-COR, Lincoln, NE	926-32219	–	1:20 000
IRDye 680RD anti-Chicken IgG	Donkey	LI-COR	926-68075	–	1:20 000

the AT8 antibody could suggest a potential diagnosis or genotype, this channel was the last to be counted in order to limit potential biases in quantification in the other channels.

A secondary analysis was performed to evaluate RPB1 mislocalization in relation to neuritic plaques in Alzheimer disease cases. Using cellSens software (Olympus, Tokyo, Japan), a circular region of interest with a radius of 0.15 mm was used to identify regions for quantification. One subset of regions was the area near neuritic plaques, in which case the circular region of interest was centered on the neuritic plaque of interest. The other subset of regions was an area relatively far from neuritic plaques, which in this case was defined as being at least 0.45 mm away from the center of a neuritic plaque. Up to 5 regions of interest centered on neuritic plaques were selected. For each case, an equivalent number of regions of interest far from neuritic plaques were randomly selected within a neuroanatomically similar region as the neuritic plaque regions of interest. For this secondary analysis, the AT8 antibody channel was viewed first to identify the neuritic plaques. Only after the regions of interest were selected was the RPB1 antibody channel viewed for quantification to minimize bias in selecting the regions of interest. Any neuron with a soma at least partially in the region of interest was considered for quantification.

Statistical Analysis

Statistical analyses were performed using Prism 8 software (GraphPad, San Diego, CA). Normality of the data was tested using the Shapiro-Wilk test. For comparison of 2 groups, the Welch's *t*-test, the Mann-Whitney test, or the Wilcoxon matched-pairs signed rank test was used, as indicated. For comparison of more than 2 groups, 1-way ANOVA was used with post-hoc comparison between groups using the Sidak test to correct for multiple comparisons. For correlations, a simple linear regression was used demonstrate the overall trend of the data, and correlation analysis was performed with Spearman's rank correlation. Comparisons were considered statistically significant at an α-level of <0.05.

Data Sharing

The data that support the findings of this study will be made available upon reasonable request to the corresponding author.

RESULTS

The phospho-specificity of the antibodies for the RPB1 CTD, the 3E8 antibody for the Ser5P epitope, and the 3E10 antibody for the Ser2P epitope, were determined by dephosphorylation of human Alzheimer disease hippocampus homogenate with lambda phosphatase. Both antibodies produced a single band on the Western blot of the hippocampal homogenate at ~200 kDa (Supplementary Data Fig. S1). There was a dose-dependent reduction in qualitative band intensity with increasing lambda phosphatase treatment, with treatment of 2000 units of lambda phosphatase resulting in complete loss of the band for both the 3E8 (Supplementary Data Fig. S1A) and 3E10 antibodies (Supplementary Data Fig. S1B). However, there was no effect of lambda phosphatase treatment on the qualitative band intensity of the GAPDH loading control (Supplementary Data Fig. S1).

In human control CA1 neurons, the staining pattern for RPB1 CTD Ser5P (using the 3E8 antibody) demonstrated a largely nuclear pattern, with most of the punctate staining distributed throughout nuclei in regions of relatively low DAPI signal (Fig. 1A), possibly representing areas of euchromatin (14). While Alzheimer disease cases also showed a similar nuclear staining pattern, there was additionally notable 3E8 staining in the cytoplasm in some CA1 neurons. This frequently occurred in neurons positive for AT8, a phospho-tau antibody used as a marker for pathologic tau; this occurred even in some neurons that did not have a classic neurofibrillary tangle morphology (Fig. 1A). Quantification of neurons with cytoplasmic 3E8 staining revealed a statistically significant difference between the number of neurons with cytoplasmic 3E8 staining in control compared to Alzheimer disease cases ($p = 0.0015$, Fig. 1B). Of note, the 2 control cases that had the highest number of neurons with cytoplasmic 3E8 were noted to both be Braak stage II cases. These observations suggested a possible relationship between cytoplasmic 3E8 staining and pathologic changes in tau. Indeed, the number of neurons with cytoplasmic 3E8 staining in a case was signifi-

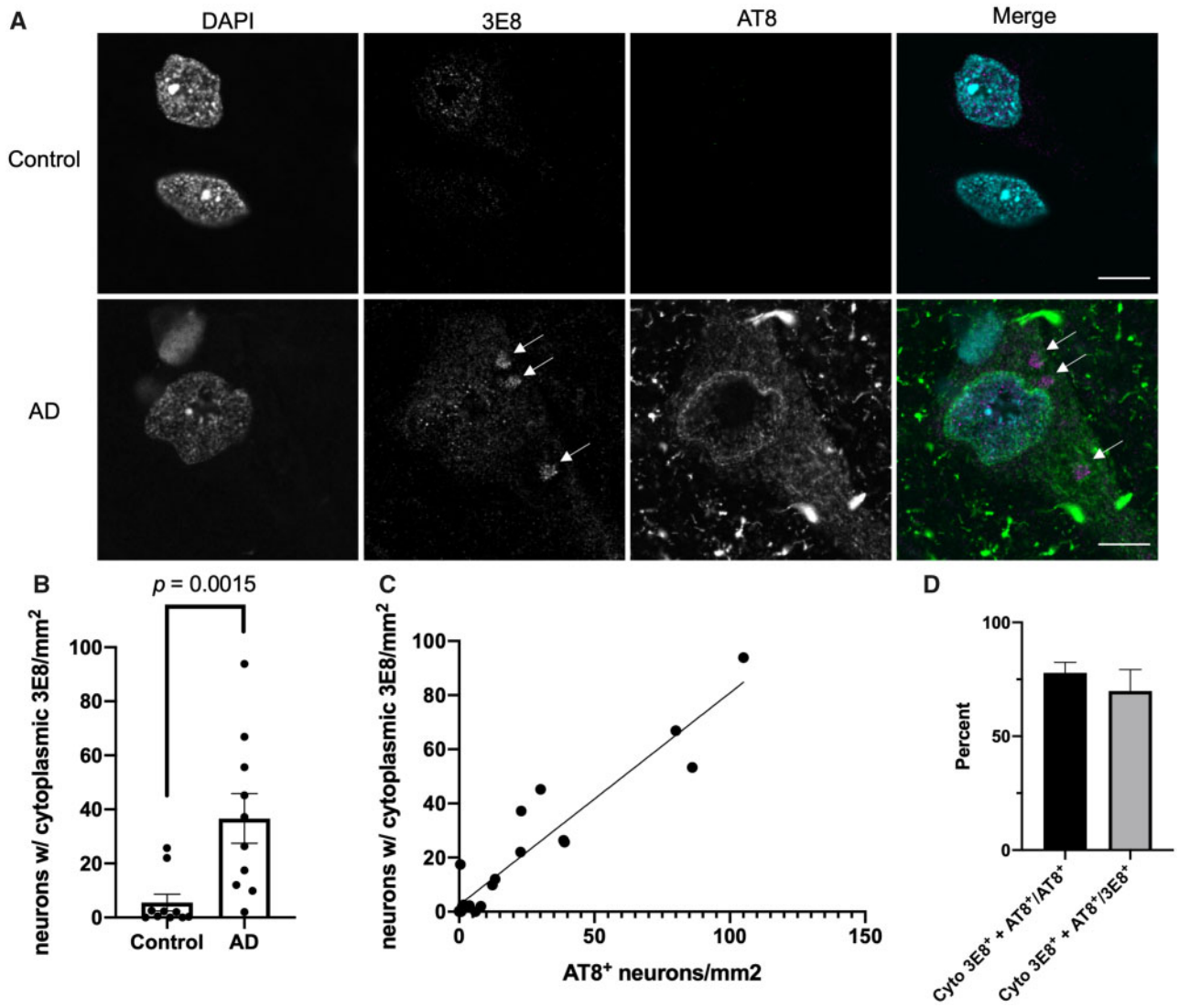

FIGURE 1. RPB1 phosphorylated at CTD serine 5 is mislocalized to the neuronal cytoplasm in Alzheimer disease. **(A)** Confocal images of control and Alzheimer disease hippocampus (CA1) stained by immunofluorescence for RPB1 CTD Ser5P (3E8 antibody, magenta in merged image) and phospho-tau (AT8 antibody, green in merged image) with nuclei counterstained by DAPI (cyan in merged image). Scale bar = 10 μm. Arrows indicate cytoplasmic 3E8 staining. **(B)** Quantification of the number of neurons with cytoplasmic 3E8 staining/mm^2 of hippocampus (CA1) in control versus Alzheimer disease cases. The individual values for each case are plotted, with the bar graph representing the mean and error bars representing the standard error of the mean (SEM) for each group. Groups were compared with the Mann-Whitney test. **(C)** Correlation of the number of neurons with cytoplasmic 3E8 staining/mm^2 with the number of AT8$^+$ neurons/mm^2. The line represents the best fit simple linear regression of the data. Spearman $r = 0.8618$, $p < 0.0001$. **(D)** Percentage of neurons in Alzheimer disease cases containing both cytoplasmic 3E8 staining and AT8 (cyto 3E8$^+$ + AT8$^+$) among neurons staining for AT8 (AT8$^+$) or 3E8 (3E8$^+$). Error bar represents SEM.

cantly correlated with the number of neurons positive for AT8 (Spearman $r = 0.8618$, $p < 0.0001$, Fig. 1C). Consistent with this observation, an average of 77.9% of AT8-positive CA1 neurons in Alzheimer disease also exhibited cytoplasmic 3E8 staining, and an average of 69.9% of CA1 neurons with cytoplasmic mislocalization of 3E8 also exhibited AT8 staining (Fig. 1D). An evaluation of sex differences with respect to the cytoplasmic mislocalization of 3E8 revealed significantly more males with the cytoplasmic mislocalization of 3E8 among controls (Supplementary Data Fig. S2A), though this was confounded by the fact that the 3 Braak stage II subjects included were all male (Table 2). No difference was observed between females and males in the Alzheimer disease cohort (Supplementary Data Fig. S2B). A secondary analysis of the relationship between neuritic plaques and the number of cells with cytoplasmic 3E8 mislocalization in Alzheimer disease cases showed no difference between regions of interest near and far from neuritic plaques (Supplementary Data Fig. S2C).

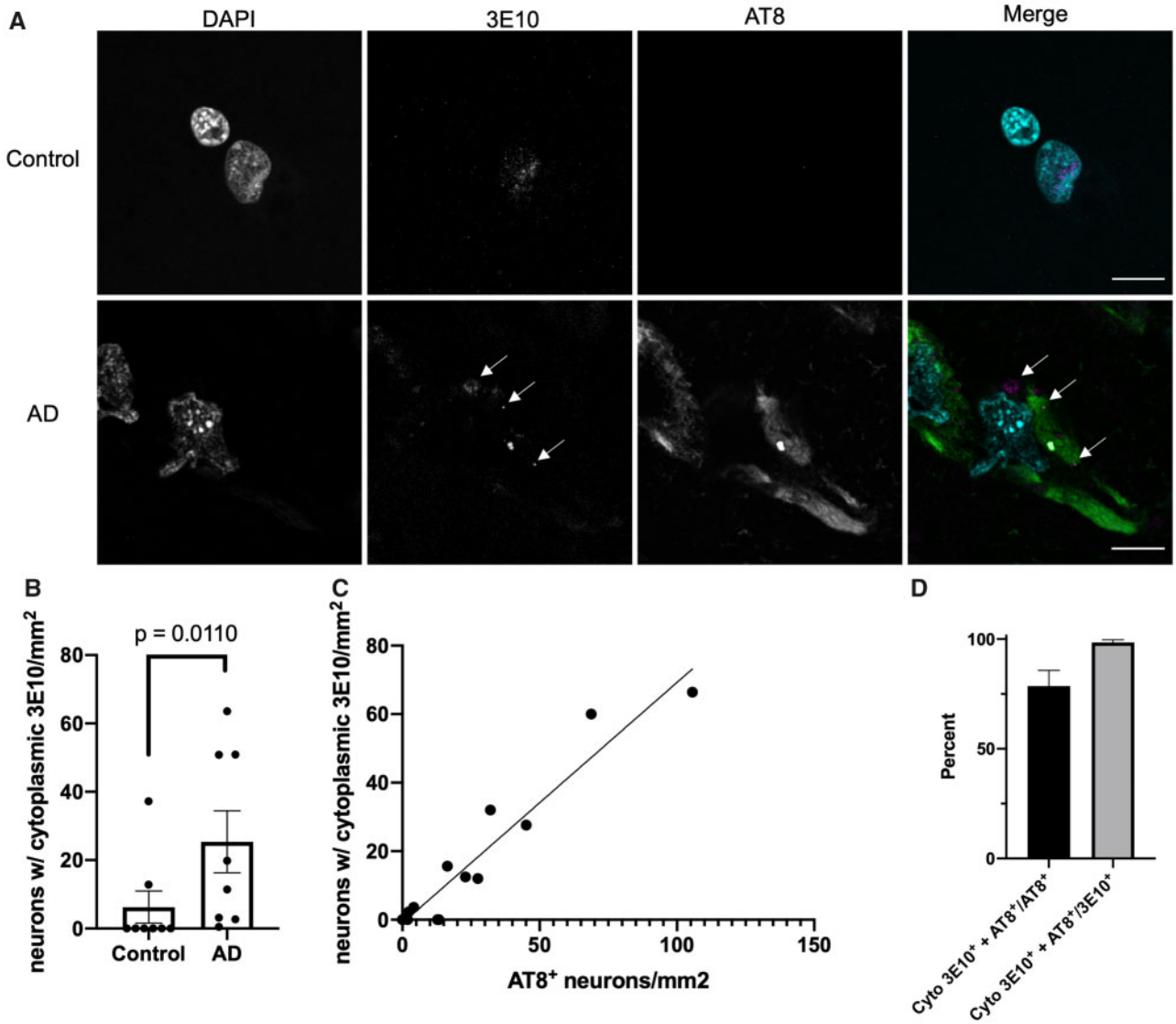

FIGURE 2. RPB1 phosphorylated at CTD serine 2 is mislocalized to the neuronal cytoplasm in Alzheimer disease. **(A)** Confocal images of control and Alzheimer disease hippocampus (CA1) stained by immunofluorescence for RPB1 CTD Ser2P (3E10 antibody, magenta in merged image) and phospho-tau (AT8 antibody, green in merged image) with nuclei counterstained by DAPI (cyan in merged image). Scale bar = 10 μm. Arrows indicate cytoplasmic 3E10 staining. **(B)** Quantification of the number of neurons with cytoplasmic 3E10 staining/mm^2 of hippocampus (CA1) in control versus Alzheimer disease cases. The individual values for each case are plotted, with the bar graph representing the mean and error bars representing the SEM for each group. Groups were compared with the Mann-Whitney test. **(C)** Correlation of the number of neurons with cytoplasmic 3E10 staining/mm^2 with the number of AT8$^+$ neurons/mm^2. The line represents the best fit simple linear regression of the data. Spearman $r = 0.8693$, $p < 0.0001$. **(D)** Percentage of neurons in Alzheimer disease cases containing both cytoplasmic 3E10 staining and AT8 (cyto 3E10$^+$ + AT8$^+$) among neurons staining for AT8 (AT8$^+$) or 3E10 (3E10$^+$). Error bar represents SEM.

Since RPB1 CTD Ser2P has previously been shown to be mislocalized in Alzheimer disease (7), we also examined this phosphoepitope. The staining pattern for RPB1 CTD Ser2P (using the 3E10 antibody) showed a similar nuclear-predominant staining in control CA1 neurons (Fig. 2A). For CA1 neurons in Alzheimer disease, the 3E10 staining also demonstrated cytoplasmic accumulations (Fig. 2A). Similar to what was observed with 3E8 staining, there was a statistically significant difference in the number of neurons with cytoplasmic 3E10 staining when control and Alzheimer disease cases ($p = 0.0110$, Fig. 2B). Likewise, there was a significant correlation between the number of cells with cytoplasmic 3E10 staining and the number of AT8-positive neurons (Spearman $r = 0.8693$, $p < 0.0001$, Fig. 2C). Among CA1 neurons in Alzheimer disease, an average of 78.5% of AT8-positive neurons also showed cytoplasmic 3E10 staining and an average of 98.5% of neurons with cytoplasmic 3E10 staining exhibited AT8-positivity (Fig. 2D). An evaluation of sex differences

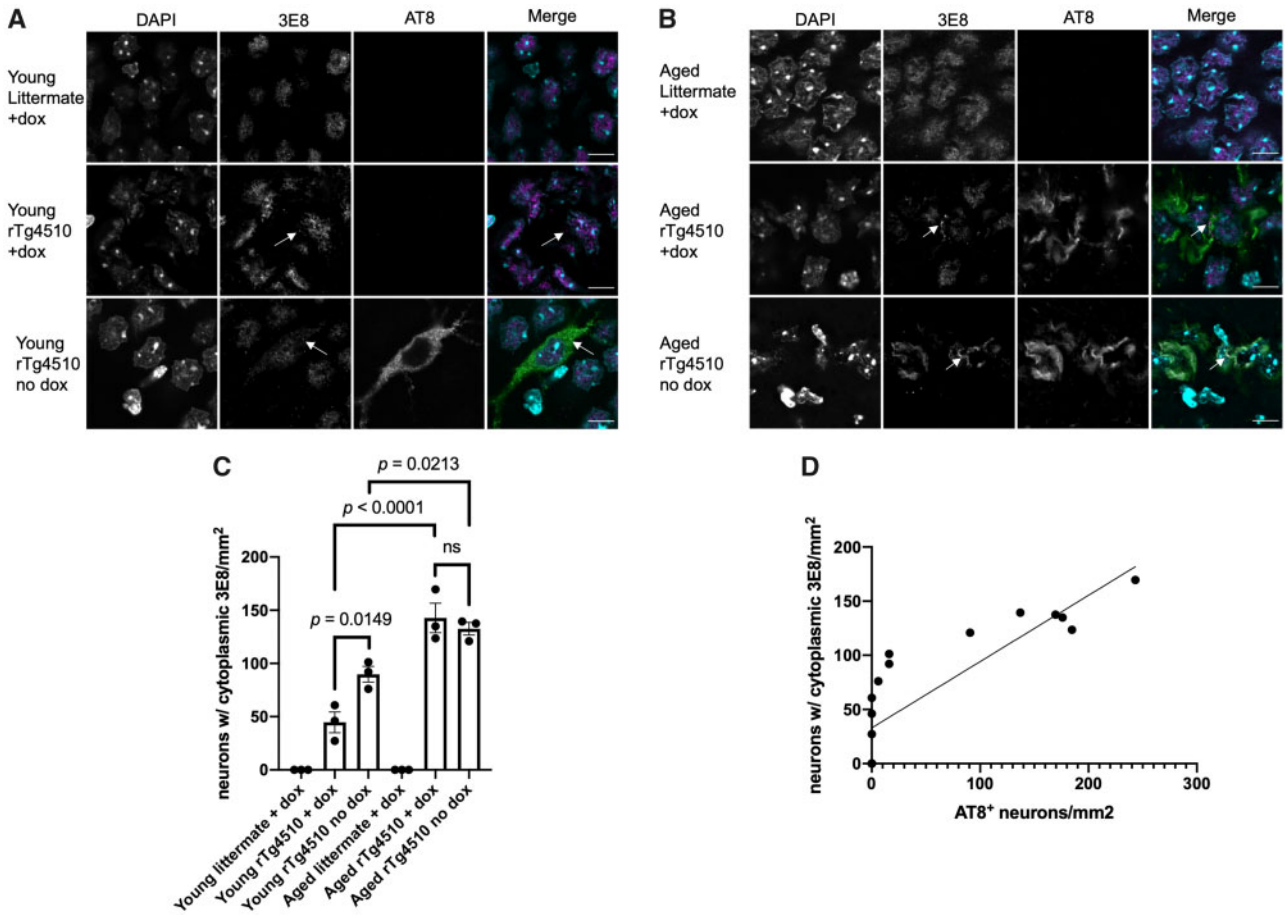

FIGURE 3. RPB1 phosphorylated at CTD serine 5 is mislocalized to the neuronal cytoplasm in rTg4510 mice in an age- and tau-dependent manner. **(A)** Confocal images of hippocampus (CA1) of young (2.5 months) rTg4510 mice ± doxycycline (dox) treatment and nontau transgenic littermates stained by immunofluorescence for RPB1 CTD Ser5P (3E8 antibody, magenta in merged image) and phospho-tau (AT8 antibody, green in merged image) with nuclei counterstained by DAPI (cyan in merged image). Scale bar = 10 μm. Arrows indicate cytoplasmic 3E8 staining. **(B)** Confocal images of hippocampus (CA1) of aged (8.5- to 10-month) rTg4510 mice ± doxycycline (dox) treatment and nontau transgenic littermates stained by immunofluorescence for RPB1 CTD Ser5P (3E8 antibody, magenta in merged image) and phospho-tau (AT8 antibody, green in merged image) with nuclei counterstained by DAPI (cyan in merged image). Scale bar = 10 μm. Arrows indicate cytoplasmic 3E8 staining. **(C)** Quantification of the number of neurons with cytoplasmic 3E8 staining/mm^2 of hippocampus (CA1) young and aged rTg4510 mice ± doxycycline (dox) treatment and nontau transgenic littermates. The individual values for each group are plotted, with the bar graph representing the mean and error bars representing the SEM for each group. Groups were compared with a 1-way ANOVA with post-hoc subgroup testing using the Sidak test to correct for multiple comparisons. Corrected p values are reported. ns = not significant. **(D)** Correlation of the number of neurons with cytoplasmic 3E8 staining/mm^2 with the number of AT8$^+$ neurons/mm^2. The line represents the best fit simple linear regression of the data. Spearman r = 0.9304, p < 0.0001.

with respect to cytoplasmic 3E10 staining revealed no difference between females and males (Supplementary Data Fig. S3A, B). A secondary analysis of 3E10 mislocalization in relation to neuritic plaques showed no difference in regions of interest near and far from neuritic plaques (Supplementary Data Fig. S3C).

While these data suggest a relationship between cytoplasmic RPB1 accumulation and pathologic tau, they do not provide information as to whether these events are causally related or only correlated. In order to test the hypothesis that pathologic tau can cause the accumulation of cytoplasmic RPB1, we used to the rTg4510 mouse model, in which the expression of pathologic human tau with the P301L mutation can be suppressed by administration of doxycycline (12). This model system also allowed for assessing the contribution of age to the phenomenon of cytoplasmic RPB1 accumulation.

As expected, for both young (2.5-month-old) and aged (8.5- to 10-month-old) non-tau transgenic littermates (control mice), the staining pattern for Rpb1 CTD Ser5P (using the 3E8 antibody) in CA1 neurons was limited to the nucleus (Fig. 3A, B), in accord with the data observed in the human control cases. Although argyrophilic tangle-like inclusions form in the hippocampus of rTg4510 mice at approximately 5.5 months of age (12), some AT8-positive hippocampal neu-

rons were present by 2.5 months of age (Fig. 3A). Even in young rTg4510 mice, some cytoplasmic 3E8 staining was evident (Fig. 3A), in a pattern similar to that seen in Alzheimer disease cases (Fig. 1A). In aged rTg4510 mice, which have numerous AT8-positive neurons in CA1, the cytoplasmic 3E8 staining pattern was even more robust and took on a more curvilinear morphology closely associated with the phospho-tau AT8 staining pattern, though some discrete punctate staining was also observed (Fig. 3B).

The causative effect of pathologic tau was evaluated by suppressing transgenic tau expression in rTg4510 mice by 6 weeks of doxycycline treatment. The cytoplasmic staining pattern of the 3E8 antibody was present even in young doxycycline-treated rTg4510 mice, which did not display staining for phospho-tau with the AT8 antibody (Fig. 3A).

In the aged doxycycline-treated rTg4510 mice, suppression of transgene expression for 6 weeks did not eliminate the AT8-positive tau aggregates in hippocampal neurons, consistent with previous reports (12). In these mice, the cytoplasmic 3E8 had a more punctate appearance that was somewhat distinct from the AT8 staining pattern (Fig. 3B), in contrast to the curvilinear morphology described above in aged untreated rTg4510 mice.

Aged rTg4510 mice had significantly higher numbers of neurons with cytoplasmic 3E8 staining compared to young rTg4510 in both doxycycline-treated and -untreated mice ($p < 0.0001$ or $p = 0.0213$, respectively, Fig. 3C). In young rTg4510 mice, suppression of tau transgene expression by 6 weeks of doxycycline treatment led to a significant reduction in the number of neurons with cytoplasmic 3E8 staining compared to rTg4510 mice expressing the tau transgene ($p = 0.0149$, Fig. 3C). For aged rTg4510 mice, in which an established population of neurons with tau inclusions exists regardless of doxycycline treatment (12), no significant difference was observed between doxycycline-treated and untreated rTg4510 mice (Fig. 3C). In examining the young and aged rTg4510 mice with or without doxycycline treatment, there was a significant correlation between the number of neurons with cytoplasmic 3E8 staining and the number of neurons with AT8 staining (Spearman $r = 0.9304$, $p < 0.0001$, Fig. 3D).

Staining for Rpb1 CTD Ser2P (using the 3E10 antibody) revealed a nuclear localization in CA1 neurons for both young and aged non-tau transgenic littermates (Fig. 4A, B). Cytoplasmic 3E10 staining was detected in young and aged Tg4510 mice (Fig. 4A, B). In contrast to 3E8 staining, young doxycycline-treated rTg4510 mice did not have evidence of cytoplasmic 3E10 staining in CA1 neurons (Fig. 4A). However, cytoplasmic 3E10 staining was observed in aged doxycycline-treated rTg4510 mice (Fig. 4B).

In contrast to the 3E8 staining, the number of neurons with cytoplasmic 3E10 staining was not significantly different between young doxycycline-treated and untreated rTg4510 mice (Fig. 4C), as one of the doxycycline-treated rTg4510 mice did not have any cytoplasmic 3E10 staining. There was also no significant difference between aged doxycycline-treated and untreated rTg4510 mice (Fig. 4C). However, an age-dependent difference was seen in the number of CA1 neurons with cytoplasmic 3E10 staining, with aged rTg4510 mice having significantly higher numbers of neurons with cytoplasmic 3E10 staining compared to young rTg4510 in both doxycycline-treated or -untreated mice ($p = 0.0045$ or $p = 0.0128$, respectively, Fig. 4C). The number of neurons with cytoplasmic 3E10 staining was significantly correlated with the number of neurons with AT8 staining (Spearman $r = 0.9271$, $p < 0.0001$, Fig. 4D).

DISCUSSION

The immunofluorescent staining for RPB1 in this study is consistent with other reports (6, 7) that RPB1, and specifically RPB1 CTD Ser5P and Ser2P (Figs. 1 and 2, respectively), is mislocalized from the nucleus to the cytoplasm of CA1 neurons in Alzheimer disease. This is in contrast to control neurons, in which the staining was nuclear, particularly in punctate areas corresponding to regions of less intense DAPI staining (Figs. 1A and 2A). These areas may represent regions of euchromatin where transcription is occurring, as RPB1 CTD Ser5P and Ser2P are marks of active transcription (10, 15) and since heterochromatin stains with DAPI more densely than euchromatin (14). Alternatively, they may represent nuclear speckles, as RNA polymerase II has been described as a component of nuclear speckles (16).

The present study adds to the existing literature about cytoplasmic RPB1 in Alzheimer disease by explicitly examining a link between cytoplasmic RPB1 accumulation and the presence of pathologic tau. The number of neurons in the CA1 region of the hippocampus with cytoplasmic RPB1 CTD Ser5P and Ser2P is positively correlated with the number of $AT8^+$ neurons in that region (Figs. 1C and 2C, respectively). We used the rTg4510 mouse model, in which the expression of pathologic tau can be regulated (12) to examine (1) whether tau (as opposed to another change in neurons in Alzheimer disease) impacts Rpb1 localization, (2) if aging contributes to cytoplasmic Rpb1 accumulation, and (3) whether suppression of tau transgene expression could prevent the cytoplasmic accumulation of Rpb1.

The presence of cytoplasmic accumulation of Rpb1 in CA1 neurons in rTg4510 mice but not non-transgenic control littermates (Figs. 3 and 4), suggests pathologic tau contributes to the cytoplasmic mislocalization of Rpb1. In the rTg4510 mouse model, the transgene insertion has disrupted *Fgf14* and 5 other genes (17), so it is possible these changes could also contribute to this phenotype. However, the fact that suppression of the tau transgene expression partially rescues the mislocalization of Rpb1 CTD Ser5P in rTg4510 mice (Fig. 3C) does suggest pathological tau contributes to the mislocalzation of Rpb1.

In the rTg4510 model, the cytoplasmic mislocalization of Rpb1 was age-dependent, with aged rTg4510 mice having significantly more neurons with mislocalized Rpb1 than young rTg4510 mice (Figs. 3C and 4C). Suppression of pathologic tau expression for 6 weeks was insufficient to significantly reduce the number of neurons with cytoplasmic Rpb1 in aged rTg4510 mice (Figs. 3C and 4C). One possible explanation for this observation is that if the cytoplasmic Rpb1 forms an aggregate over time and at the 8.5- to 10-month time point, a reduction in pathologic tau expression may not be able to impact the number of Rpb1 aggregates that have already

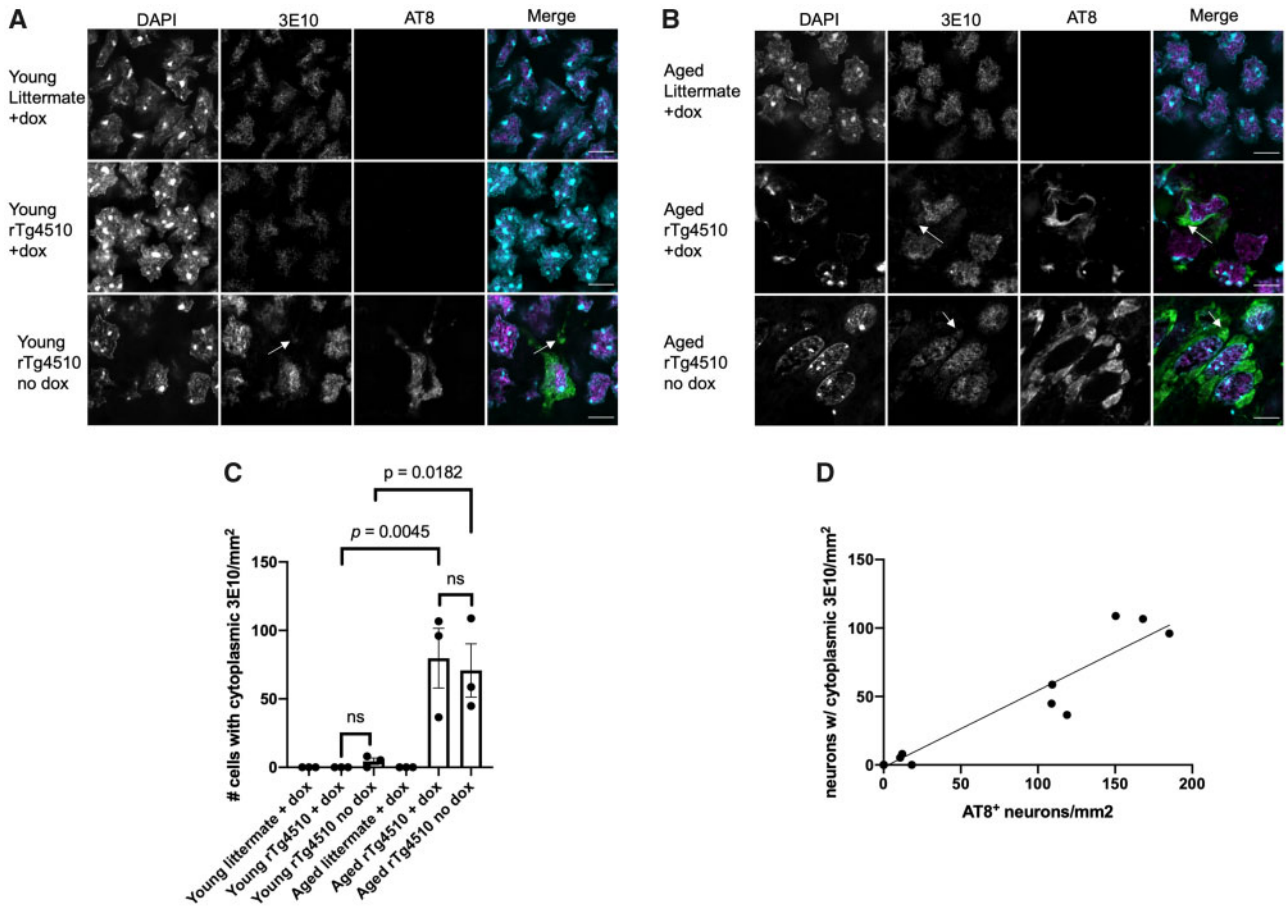

FIGURE 4. RPB1 phosphorylated at CTD serine 2 is mislocalized to the neuronal cytoplasm in rTg4510 mice in an age-dependent manner. **(A)** Confocal images of hippocampus (CA1) of young (2.5 months) rTg4510 mice ± doxycycline (dox) treatment and nontau transgenic littermates stained by immunofluorescence for RPB1 CTD Ser2P (3E10 antibody, magenta in merged image) and phospho-tau (AT8 antibody, green in merged image) with nuclei counterstained by DAPI (cyan in merged image). Scale bar = 10 μm. Arrows indicate cytoplasmic 3E10 staining. **(B)** Confocal images of hippocampus (CA1) of aged (8.5- to 10-month) rTg4510 mice ± doxycycline (dox) treatment and nontau transgenic littermates stained by immunofluorescence for RPB1 CTD Ser2P (3E10 antibody, magenta in merged image) and phospho-tau (AT8 antibody, green in merged image) with nuclei counterstained by DAPI (cyan in merged image). Scale bar = 10 μm. Arrows indicate cytoplasmic 3E10 staining. **(C)** Quantification of the number of neurons with cytoplasmic 3E10 staining/mm^2 of hippocampus (CA1) young and aged rTg4510 mice ± doxycycline (dox) treatment and non-tau transgenic littermates. The individual values for each group are plotted, with the bar graph representing the mean and error bars representing the SEM for each group. Groups were compared with a 1-way ANOVA with post-hoc subgroup testing using the Sidak test to correct for multiple comparisons. Corrected p values are reported. ns = not significant. **(D)** Correlation of the number of neurons with cytoplasmic 3E10 staining/mm^2 with the number of AT8$^+$ neurons/mm^2. The line represents the best fit simple linear regression of the data. Spearman r = 0.9271, $p < 0.0001$.

formed. While suppression of pathologic tau expression did not reduce the number of neurons with cytoplasmic Rpb1 CTD Ser5P, there was a notable change in morphology. The aged rTg4510 mice with pathologic tau expression suppressed by doxycycline treatment displayed mostly punctate cytoplasmic Rpb1 staining, similar to those seen in young rTg4510 mice, whereas those with continued pathologic tau expression began to show curvilinear staining that generally corresponded with regions of AT8 staining. This may indicate incorporation or close association of Rpb1 CTD Ser5P with pathologic tau aggregates.

The young doxycycline-treated rTg4510 mice did not have AT8-positive tau aggregation, but they did reveal cytoplasmic accumulation of Rpb1 CTD Ser5P (Fig. 3A), which is consistent with previous speculation that cytoplasmic RPB1 accumulation in Alzheimer disease is an early phenomenon in the pathophysiology of Alzheimer disease, including in neurons without histopathologic evidence of overt tau aggregation (7). In contrast to Rpb1 CTD Ser5P, young doxycycline-treated rTg4510 mice did not display cytoplasmic staining of Rpb1 CTD Ser2P (Fig. 4A, C). For young untreated rTg4510 mice, there were many fewer CA1 neurons with cytoplasmic staining for Rpb1 CTD Ser2P than for staining for Rpb1 CTD Ser5P (Figs. 4C vs 3C). In fact, 1 of the 3 animals in this group completely lacked cytoplasmic staining for Rpb1 CTD Ser2P. While the reason for this difference between the 2 phosphoepi-

topes is not entirely clear from this study, one possible explanation is that the cytoplasmic staining for the Rpb1 CTD Ser2P develops later than that for Rpb1 CTD Ser5P.

Suppression of tau transgene expression by doxycycline administration for 6 weeks significantly reduced the number of neurons with cytoplasmic Rpb1 CTD Ser5P accumulation in young rTg4510 mice (Fig. 3C). There were few neurons with cytoplasmic accumulation of Rpb1 CTD Ser2P in young rTg4510 mice, and suppression of tau transgene suppression did not significantly change this (Fig. 4C). In aged rTg4510 mice, suppression of tau transgene expression did not significantly alter the number of neurons with cytoplasmic accumulations of either Rpb1 CTD Ser5P or Rpb1 CTD Ser2P (Figs. 3C and 4C). The fact that suppression of tau transgene expression in young rTg4510 mice reduces the number of neurons with cytoplasmic Rpb1 CTD Ser5P mislocalization suggests a causal role for pathologic tau in the cytoplasmic mislocalization of RPB1 in Alzheimer disease. This also provides some clues as to some general characteristics of the tau species that may mediate this effect. The suppression of active tau expression in young rTg4510 mice (2.5-months old) at an age in which tangle-like tau inclusions have not yet developed (12), indicates soluble and/or oligomeric tau species, rather than insoluble fibrils, are likely responsible.

While this study does not examine the mechanism by which the cytoplasmic mislocalization of RPB1 occurs in Alzheimer disease, there are several potential causes to consider. RPB1 is initially translated in the cytoplasm and is incorporated with other components, including 1 with a nuclear localization signal, into the core RNA polymerase II complex in the cytoplasm. The assembled RNA polymerase II complex is then imported to the nucleus via the nuclear pore complex (18). Disruption of any of these steps following translation to nuclear import could result in RPB1 accumulation in the cytoplasm. In *Saccharomyces cerevisiae,* Not5 has been shown to aid in RNA polymerase II assembly, and deletion of its homolog, *CNOT3*, in *Drosophila melanogaster* results in cytoplasmic accumulation of Rpb1 (19). The requirement for RNA polymerase II complex assembly in the cytoplasm prior to nuclear import has also been demonstrated in human U2OS cells, in which knockdown of any other core RNA polymerase II complex component results in the cytoplasmic accumulation of RPB1 (20). Because the fully assembled RNA polymerase II complex must be imported to the nuclear via the nuclear pore complex (18), impairment of this step in nuclear import could also potentially result in cytoplasmic accumulation of RPB1. Of note, recent studies have suggested that pathologic tau can disrupt the nuclear envelope and interfere with nucleocytoplasmic transport (5, 21, 22). Work from our lab has indicated that one possible contributor to the disrupted nucleocytoplasmic transport is mediated by the binding of soluble oligomeric, nonfibrillar tau to nucleoporin 98 (NUP98), a component of the nuclear pore complex (5). Another possible way tau could contribute to the mislocalization of RPB1 is if RPB1 forms cytoplasmic aggregates physically associated with pathologic tau in Alzheimer disease. If this occurred, the aggregated subset of RPB1 may be unavailable for assembly and transport into the nucleus. Since suppression of soluble tau expression in young rTg4510 mice reduces the number of neurons with cytoplasmic Rpb1 accumulation (Fig. 3C) and since aged rTg4510 mice demonstrate cytoplasmic Rpb1 accumulations and phospho-tau aggregates in close proximity (Figs. 3B and 4B), we speculate that both mechanisms could be at play in an age-dependent manner in a "two-hit" model. A soluble or early aggregate form of tau could promote the cytoplasmic mislocalization at an early time point, possibly due to disruption of nucleocytoplasmic transport, and then RPB1 associates with tau aggregates in the cytoplasm, stabilizing its cytoplasmic localization, and further preventing its ability to be transported into the nucleus.

Given the essential role of RPB1 as the catalytic subunit of RNA polymerase II, which is responsible for the transcription of mRNA and some small RNAs from nuclear DNA (8), the mislocalization of RPB1 to the cytoplasm may have some impact on neuronal physiology. Previous work has shown that in Alzheimer disease, neurons with cytoplasmic RPB1 have reduced mRNA based on in situ hybridization with a poly-T probe compared to neurons without cytoplasmic RPB1 (7). More recently, single-nucleus RNA sequencing in Alzheimer disease and control prefrontal cortex has revealed that among the differentially expressed genes, there is a strong trend toward a general repression of gene expression in in neurons in Alzheimer disease (11). Since RPB1 is a critical enzyme in the generation of mRNAs, mislocalization of RPB1 could contribute to this striking alteration in neuronal physiology.

There are some limitations of this study, which must be noted. Fluorescent imaging of brain tissue is complicated by autofluorescence from substances such as lipofuscin. Lipofuscin accumulates in neurons and has fluorescent properties, with a broad excitation and emission spectrum. We attempted to minimize the interference from tissue autofluorescence by quenching the autofluorescence with Sudan black (23). While autofluorescence could interfere with our fluorescent microscopy, we expect that this was minimal given the generally distinct staining pattern seen for the different fluorescent probes used this study. Another limitation of our study is that it was not designed to evaluate the effect of *APOE* genotype on the cytoplasmic mislocalization of RPB1. Not all of our tissue samples had an *APOE* genotype available. Of those with *APOE* genotype information available, the majority were of the ε3/ε3 genotype. One control subject had a ε2/ε3 genotype, and 1 Alzheimer disease subject had a ε3/ε4 genotype (Table 2). Further studies are needed to assess any possible contributions of *APOE* genotype to the mislocalization of RPB1 in Alzheimer disease. Additionally, this study was not designed to specifically detect sex differences in the mislocalization of RPB1. In general, no clear sex difference was observed (Supplementary Data Figs. S2A, B and S3A, B). The significant difference seen in the cytoplasmic 3E8 staining pattern in control subjects is confounded by the inclusion of 3 males with Braak stage II (Table 2), which occurred by chance. Further studies that are specifically powered to discern sex difference are needed in the future to address any effect of sex on the mislocalization of RPB1. In a secondary exploratory analysis, proximity to neuritic plaques did not seem to influence the likelihood of neurons having a cytoplasmic mislocalization of RPB1 (Supplementary Figs. S2C and S3C). The detection of neuritic plaques was based on phospho-tau staining with the

AT8 antibody in this study, and while amyloid-beta was not specifically stained in this study, the observation that proximity to neuritic plaques do not seem to influence RPB1 mislocalization implies that amyloid-beta does not influence it either. Conversely, these observations seem to suggest that RPB1 mislocalization does not influence amyloid-beta deposition or neuritic plaque formation. However, the relationship between amyloid-beta and RPB1 mislocalization was not explicitly addressed prospectively in this study, and the number of subjects included in the secondary analysis of neuritic plaques was relatively small. Therefore, further studies are needed to better determine the relationship between amyloid-beta and RPB1 mislocalization.

Overall, the experiments presented in this study link the mislocalization of RNA polymerase II subunit RPB1 with pathologic tau. We have demonstrated a statistically significant increase in the number of neurons with cytoplasmic mislocalization of RPB1 in Alzheimer disease, which is strongly correlated with phospho-tau pathological changes. To test the possibility pathologic tau causes RPB1 mislocalization, we examined whether pathologic tau overexpression the rTg4510 mouse model induced RPB1 mislocalization. We found that, indeed, mislocalization of RPB1 to the cytoplasm was observed in rTg4510 hippocampal neurons. This phenotype is age-dependent, and in the case of Rpb1 CTD Ser5P in young rTg4510 mice, it is tau-dependent. Taken together, these data suggest that the mislocalization of RPB1 is downstream of pathologic changes in tau in the pathophysiology of Alzheimer disease. This provides a foundation for further investigation into the causes and consequences of mislocalized RPB1 in Alzheimer disease, and a deeper understanding of the pathophysiology of Alzheimer disease may help explain the profound changes in mRNA expression recently described by single-nucleus RNA sequencing of neurons in Alzheimer disease.

ACKNOWLEDGEMENTS

The authors wish to thank Dr. Alberto Serrano-Pozo and Dr. Richard Young for helpful discussions regarding this study. The authors also thank Caitlin Commins, Jose Gonzalez, Patrick Dooley, and Theresa Connors for technical assistance.

REFERENCES

1. Serrano-Pozo A, Frosch MP, Masliah E, Hyman BT. Neuropathological alterations in Alzheimer disease. Cold Spring Harb Perspect Med 2011; 1:a006189
2. Binder LI. The distribution of tau in the mammalian central nervous system. J Cell Biol 1985;101:1371–8
3. Kowall NW, Kosik KS. Axonal disruption and aberrant localization of tau protein characterize the neuropil pathology of Alzheimer's disease. Ann Neurol 1987;22:639–43
4. Sheffield LG, Miskiewicz HB, Tannenbaum LB, et al. Nuclear pore complex proteins in Alzheimer disease. J Neuropathol Exp Neurol 2006;65: 45–54
5. Eftekharzadeh B, Daigle JG, Kapinos LE, et al. Tau protein disrupts nucleocytoplasmic transport in Alzheimer's disease. Neuron 2018;99: 925–40.e7
6. Mastroeni D, Chouliaras L, Grover A, et al. Reduced RAN expression and disrupted transport between cytoplasm and nucleus; a key event in Alzheimer's disease pathophysiology. PLoS One 2013;8:e53349
7. Husseman JW, Hallows JL, Bregman DB, et al. Hyperphosphorylation of RNA polymerase II and reduced neuronal RNA levels precede neurofibrillary tangles in Alzheimer disease. J Neuropathol Exp Neurol 2001; 60:1219–32
8. Svetlov V, Nudler E. Basic mechanism of transcription by RNA polymerase II. Biochimica et Biophysica Acta 2013;1829:20–8
9. Boehning M, Dugast-Darzacq C, Rankovic M, et al. RNA polymerase II clustering through carboxy-terminal domain phase separation. Nat Struct Mol Biol 2018;25:833–40
10. Harlen KM, Churchman LS. The code and beyond: transcription regulation by the RNA polymerase II carboxy-terminal domain. Nat Rev Mol Cell Biol 2017;18:263–73
11. Mathys H, Davila-Velderrain J, Peng Z, et al. Single-cell transcriptomic analysis of Alzheimer's disease. Nature 2019;570:332–7
12. SantaCruz K. Tau Suppression in a neurodegenerative mouse model improves memory function. Science 2005;309:476–81
13. Spires TL, Orne JD, SantaCruz K, et al. Region-specific dissociation of neuronal loss and neurofibrillary pathology in a mouse model of tauopathy. Am J Pathol 2006;168:1598–607
14. Quivy J-P, Roche D, Kirschner D, et al. A CAF-1 dependent pool of HP1 during heterochromatin duplication. EMBO J 2004;23:3516–26
15. Guo YE, Manteiga JC, Henninger JE, et al. Pol II phosphorylation regulates a switch between transcriptional and splicing condensates. Nature 2019;572:543–8
16. Spector DL, Lamond AI. Nuclear Speckles. Cold Spring Harbor Perspect Biol 2011;3:a000646
17. Gamache J, Benzow K, Forster C, et al. Factors other than hTau overexpression that contribute to tauopathy-like phenotype in rTg4510 mice. Nat Commun 2019;10:2479
18. Di C. Regulating the shuttling of eukaryotic RNA polymerase II. Mol Cell Biol 2011;31:3918–20
19. Villanyi Z, Ribaud V, Kassem S, et al. The Not5 subunit of the ccr4-not complex connects transcription and translation. PLoS Genet 2014;10: e1004569
20. Boulon S, Pradet-Balade B, Verheggen C, et al. HSP90 and Its R2TP/ Prefoldin-like cochaperone are involved in the cytoplasmic assembly of RNA polymerase II. Mol Cell 2010;39:912–24
21. Frost B, Bardai FH, Feany MB. Lamin dysfunction mediates neurodegeneration in tauopathies. Curr Biol 2016;26:129–36
22. Paonessa F, Evans LD, Solanki R, et al. Microtubules deform the nuclear membrane and disrupt nucleocytoplasmic transport in tau-mediated frontotemporal dementia. Cell Reports 2019;26:582–93.e5
23. Schnell SA, Staines WA, Wessendorf MW. Reduction of lipofuscin-like autofluorescence in fluorescently labeled tissue. J Histochem Cytochem 1999;47:719–30